LANGMUIR

Article pubs.acs.org/Langmuir

Statistical Mechanical Model of Gas Adsorption in a Metal-Organic Framework Harboring a Rotaxane Molecular Shuttle

Jonathan Carney, David Roundy,* and Cory M. Simon*



Cite This: Langmuir 2020, 36, 13112-13123



ACCESS I

III Metrics & More

Article Recommendations

Supporting Information

ABSTRACT: Metal-organic frameworks (MOFs) are modular and tunable nanoporous materials with applications in gas storage, separations, and sensing. Integrating flexible/ dynamic, gas-responsive components into MOFs can give them unique or enhanced adsorption properties. Here, we explore the adsorption properties that could be imparted to a MOF by a rotaxane molecular shuttle (RMS) in its pores. In the unit cell of an RMS-MOF, a macrocyclic wheel is mechanically interlocked with a strut of the MOF scaffold. The wheel shuttles between stations on the strut that are also gas adsorption sites. At a level of abstraction similar to the seminal Langmuir adsorption model, we pose and analyze a simple statistical mechanical model of gas adsorption in an RMS-MOF that



accounts for (i) wheel/gas competition for sites on the strut and (ii) gas-induced changes in the configurational entropy of the shuttling wheel. We determine how the amount of gas adsorbed, the position of the wheel, and the differential energy of adsorption depend on temperature, pressure, and the interactions of the gas and wheel with the stations on the strut. Our model reveals that, compared to a rigid, Langmuir material, the chemistry of the RMS-MOF can be tuned to render gas adsorption more or less temperature sensitive and to release more or less heat upon adsorption. The model also uncovers that, if gas-wheel competition for a station is fierce, temperature influences the position of the wheel differently depending on the amount of gas adsorbed.

INTRODUCTION

Metal-organic frameworks (MOFs) are nanoporous, crystalline materials with adsorption-based applications in storing, separating,² and sensing³ gases. MOFs are synthesized modularly by linking metals or metal clusters, serving as nodes, to organic linker molecules, serving as struts.^{4,5} Because of the abundance of compatible molecular building blocks (nodes and struts), a practically limitless number of different MOFs, with diverse properties, can be synthesized (tens of thousands thus far⁶).

The integration of dynamic and flexible components into the structures of MOFs, enabled by their synthetic adjustability, could impart them with unique or enhanced adsorption properties that are inaccessible to static, rigid materials. Already, several different modes of flexibility have been incorporated in MOFs⁸⁻¹³ and given rise to anomalous adsorption properties¹⁴ that can be exploited for engineering applications. Modes of flexibility include the rotation¹⁵ and bending ¹⁶ of linkers, hinging of the backbone of, e.g., wine-rack motifs, ¹⁷ and displacement of interdigitated or interpenetrated networks; 18 consequent anomalous adsorption properties 14 include inflections and discontinuities in gas adsorption isotherms, ¹³ intrinsic mitigation of the heat released upon adsorption, ²⁰ negative gas adsorption, ²¹ adsorption-induced contraction ²² and expansion, ²⁰ metastability, ^{23,24} and adsorption/desorption hysteresis.²⁵

Co(bdp)²⁵ is a flagship example of a flexible MOF with unique and useful adsorption properties. Co(bdp) possesses a wine-rack-like structure permissive of hinge motion. When immersed in methane gas, at low pressure, Co(bdp) adopts a collapsed, nonporous state but expands to a porous state and fills with gas at higher pressures.²⁰ This imparts Co(bdp) with several unique adsorption properties advantageous for vehicular natural gas storage and delivery.²⁰ First, the resulting stepped methane adsorption isotherm equips Co(bdp) with the highest reported methane usable capacity. Unlike rigid MOFs, Co(bdp) collapses at the discharge pressure to fully expel its cushion gas. Second, the endothermic framework expansion induced by adsorbed gas consumes a fraction of the heat released upon adsorption. This is advantageous because such heat raises the temperature of the adsorbent, diminishing its usable capacity.²⁶ Third, Co(bdp) responds to mechanical pressure by collapsing and expelling gas, offering a new means to induce gas desorption.

However, despite their appealing adsorption properties, such MOFs with pliable struts and backbones are arguably infeasible for practical applications: repeated dynamics eventually lead to structural failure and degradation. In addition, engineering challenges are associated with designing a pressure vessel that

September 26, 2020 Received: Revised: October 6, 2020 Published: October 23, 2020





accommodates the volume changes of flexible MOFs with lattice distortions. 13

A vision toward robust, high-fidelity, fixed-volume MOFs that retain dynamic complexity and exhibit adsorption properties inaccessible to rigid materials is to graft dynamic, mechanically interlocked molecules onto rigid MOFs, treated as scaffolds. 7,27-29 In contrast to MOFs with pliable struts and backbones which, subject to repeated dynamics, will rupture, mechanically interlocked molecules 30,31 can undergo repeated dynamics without breakage. In addition, as some mechanically interlocked molecules are influenced by light and electric field,²⁷ integrating mechanically interlocked components into MOF scaffolds may offer new routes to modulate gas adsorption with exotic (aside from the usual temperatureand pressure-swing) external stimuli. As an example mechanically interlocked molecule, a [2]rotaxane^{27,32-34} consists of a long molecule (the "axle") threaded through a macrocycle (the "wheel"); bulky groups at the two ends of the axle prevent the wheel from sliding off, thereby mechanically interlocking the wheel and axle. In a [2]rotaxane molecular shuttle, the wheel is free to translate along the axle, which can be decorated with functional groups that serve as "stations" for the wheel, possibly with different affinities for it. Pioneering experimental studies have demonstrated the integration of rotaxanes into MOF scaffolds, 35-46 but resultant adsorption properties have not been investigated.

Metal—organic frameworks with rotaxane molecular shuttles operating in their pores, ³⁶ RMS-MOFs (RMS = rotaxane molecular shuttle), are particularly promising for exhibiting anomalous adsorption properties, which could arise from (i) energetic effects via competition between the wheel and a gas molecule for a station on the axle and (ii) entropic effects via adsorbed gas altering the translational freedom of the wheel. In 2015, Loeb and co-workers³⁶ synthesized an RMS-MOF coined UWDM-4.²⁸ The struts of UWDM-4 are an axle of a [2]rotaxane, whose macrocyclic wheel was shown to rapidly shuttle between the two benzimidazole stations on its strut, unimpeded owing to the porosity of the MOF.³⁶ Figure 1a shows the [2]rotaxane linker used to synthesize UWDM-4. To our knowledge, UWDM-4 is the only reported RMS-MOF, and its adsorption properties have not been studied.

Herein, we formulate and analyze a simple statistical mechanical model of an RMS-MOF and its interaction with gas molecules to investigate its adsorption properties (see Figure 1b). Our goals are to fundamentally understand how the adsorption properties of an RMS-MOF are affected by (i) competition between the wheel and gas for stations/sites on the strut of the MOF and (ii) changes in the translational entropy of the shuttling wheel induced by the adsorption of gas. By formulating a useful abstraction of the RMS-MOF similar in spirit to the seminal Langmuir adsorption model, 47 we aim to illuminate potentially anomalous or enhanced adsorption properties that could be imparted by a shuttling wheel within a MOF. Compared to a rigid, single-site Langmuir material, we find that, depending on the interactions of the wheel and gas with the stations/sites, (i) adsorption in the RMS-MOF can be more or less temperature sensitive and (ii) more or less heat can be released upon adsorption. Interestingly, we also find that, if the gas fiercely competes with the wheel for a station/site, temperature changes affect the position of the wheel differently depending on the amount of gas adsorbed.

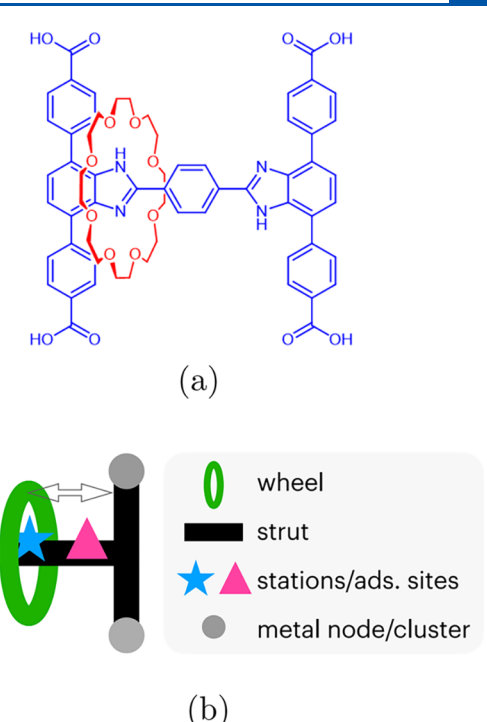


Figure 1. MOF with a rotaxane molecular shuttle operating in its pores, an RMS-MOF. (a) RMS-MOF linker used to synthesize UWDM-4 (blue: axle/strut; red: wheel), 36 which inspired our abstraction in (b). (b) Our abstraction of the unit cell of an RMS-MOF. The wheel can translate along the rotaxane axle (=the strut of the MOF), which harbors two distinct stations (\rightleftarrows and \triangle) for the wheel that also serve as adsorption sites for gas molecules. If the wheel occupies the \bigstar (\triangle) station, the \triangle (\bigstar) adsorption site is exposed to the gas.

BACKGROUND: THE LANGMUIR ADSORPTION MODEL

We first briefly review the classic, single-site Langmuir adsorption model,⁴⁷ to which we will compare our RMS-MOF model.

The unit cell of a Langmuirian MOF offers a single, independent gas adsorption site, \square (see Figure 2a). Let $n \in \{0, 1\}$ be the number of adsorbed gas particles in the unit cell, our system, and ϵ_{\square} be the energy of the gas— \square interaction. The energy of the system is then $E(n) = n\epsilon_{\square}$.

Immersed in a bath of gas at temperature T and chemical potential μ , the grand-canonical partition function of the Langmuir MOF system is

$$\xi_{L}(\mu, T) = \sum_{n \in \{0,1\}} e^{-\beta E(n) + \beta \mu n} = 1 + e^{\beta(\mu - \epsilon_{\square})}$$
(1)

with $\beta=1/(k_{\rm B}T)$ and $k_{\rm B}$ the Boltzmann constant. The expected number of adsorbed gas molecules in the Langmuir MOF is

$$\langle n \rangle_{L}(P, T) = \sum_{n \in \{0,1\}} n \frac{e^{-\beta E(n) + \beta \mu n}}{\xi_{L}} = \frac{K_{\square} \beta P}{1 + K_{\square} \beta P}$$
(2)

We arrived at eq 2 by treating the gas phase as an ideal (lattice) gas, giving a relation between the pressure P of the gas and its chemical potential μ , $\beta P = e^{\beta\mu}$ (see Section S1). The Langmuir parameter $K_{\square} \equiv e^{-\beta e_{\square}}$ is a function of temperature and describes the affinity of the gas for the \square adsorption site; the \square adsorption sites are half-occupied when the density of the

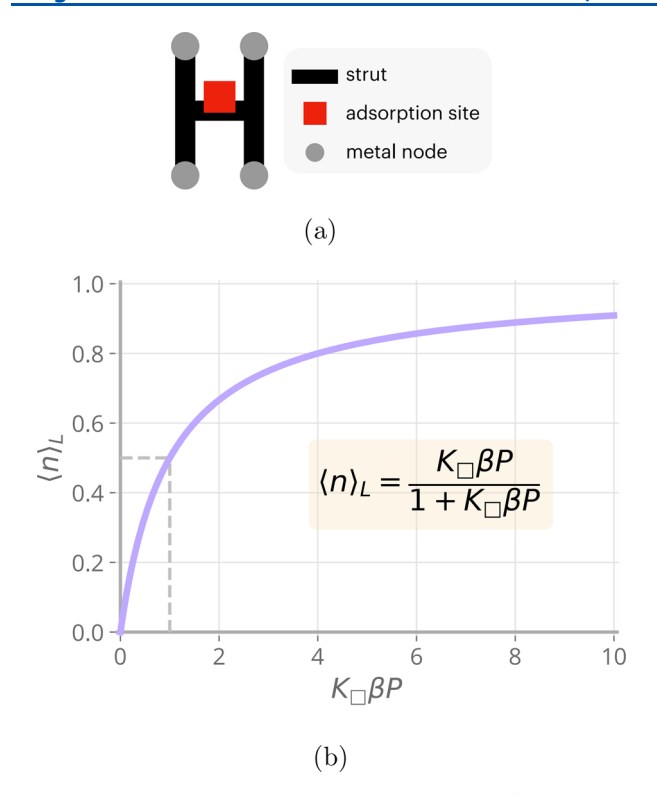


Figure 2. Single- \square -site Langmuir adsorption model. (a) Unit cell of a single-site Langmuir material offers an adsorption site, \square , with ϵ_{\square} the gas- \square interaction energy. (b) Langmuir adsorption isotherm in eq 2, with βP the density of the (ideal) bulk gas and $K_{\square} \equiv \mathrm{e}^{-\beta \epsilon_{\square}}$ the temperature-dependent Langmuir parameter. Half-saturation of the adsorption sites occurs when $K_{\square}\beta P=1$ (dashed lines).

ideal gas phase $\beta P = 1/K_{\square}$. Figure 2b shows the shape of the Langmuir adsorption isotherm in eq 2, a monotonically increasing, concave function that approaches one (full occupancy) as $K_{\square}\beta P \to \infty$. Finally, the internal energy of the Langmuirian unit cell is, intuitively, the product of the occupancy and the gas— \square interaction

$$\langle E \rangle_{L}(P, T) = \sum_{n \in \{0,1\}} E(n) \frac{e^{-\beta E(n) + \beta \mu n}}{\xi_{L}} = \epsilon_{\square} \langle n \rangle_{L}(\mu, T)$$
(3)

This gives a differential energy of adsorption $\partial \langle E \rangle_{\rm L}/\partial \langle n \rangle_{\rm L} = \epsilon_{\square}.$

ABSTRACTING GAS ADSORPTION IN AN RMS-MOF

We now formulate a toy statistical mechanical model of (pure) gas adsorption in a MOF with a rotaxane molecular shuttle operating in its pores, i.e., in an RMS-MOF. Figure 1b shows our modeling abstraction of the unit cell of the RMS-MOF structure, inspired by UWDM-4. The (bistable) rotaxane strut of the RMS-MOF presents two distinct binding sites, \approx and \triangle , that serve as: (i) stations for the shuttling, macrocyclic wheel mechanically interlocked with the strut and (ii) adsorption sites for the gas. Because the wheel sterically excludes gas, the position of the wheel determines which adsorption site is exposed to the gas. We take the RMS-MOF scaffold as rigid, imposing a constant volume.

Space of Microstates. We begin by specifying the space of possible microstates of the RMS-MOF—gas system. We define

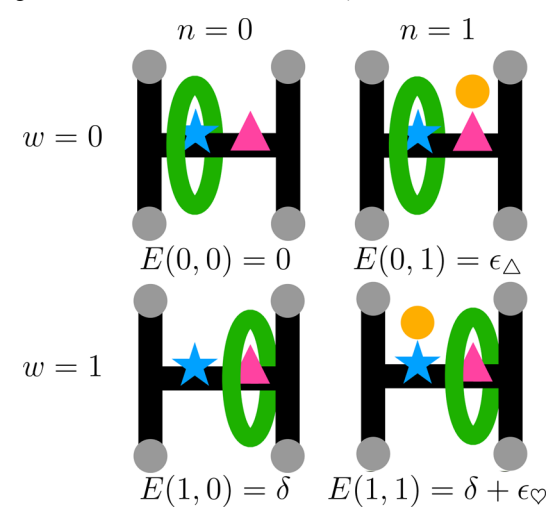
the system as one unit cell of the RMS-MOF crystal shown in Figure 1b. We treat this as an independent system, thereby neglecting interactions of gas molecules and wheels with those in neighboring unit cells.

The wheel. The wheel can adopt two possible microstates: it sits at either the \Leftrightarrow or \triangle station. Let $w \in \{0, 1\} \equiv W$ denote the microstate of the wheel on the strut $(w = 0 \Rightarrow$ wheel on \Leftrightarrow , $w = 1 \Rightarrow$ wheel on \triangle).

The gas. The RMS-MOF unit cell can fit only one gas molecule inside. Let $n \in \{0, 1\} \equiv \mathcal{N}$ be the number of gas molecules adsorbed. If n = 1, the site on which the gas molecule is adsorbed is determined by the state of the wheel, w. If w = 0, the \triangle site is exposed to the gas. If w = 1, the \Leftrightarrow site is exposed to the gas.

The RMS-MOF-gas system. The set of four possible microstates of the RMS-MOF-gas system, $\mathcal{W} \times \mathcal{N}$, is enumerated in Table 1.

Table 1. List of Microstates, $W \times N$, and Associated Energies for the RMS-MOF–Gas System^a



^aOrange sphere represents an adsorbed gas molecule.

Energy of the Microstates. Next, we prescribe the energy of each microstate of the RMS-MOF-gas system. The $\not\approx$ station is the ground state of the wheel, with δ the energetic penalty for the wheel to reside at the \triangle station instead. A gas molecule adsorbed on the $\not\approx$ and \triangle adsorption site experiences an energy of $\epsilon_{\not\approx}$ and ϵ_{\triangle} , respectively, owing to (van der Waals, electrostatic, etc.) interactions with the site. The energy E of microstate $(w, n) \in \mathcal{W} \times \mathcal{N}$ is then

$$E(w, n) = w\delta + n[w\epsilon_{\pm} + (1 - w)\epsilon_{\triangle}]$$
(4)

The first and second term arise from wheel—station and gas—station interactions, respectively. Table 1 illustrates the energy prescription in eq 4. Table 2 summarizes model parameters.

RMS-MOF Material Space. Owing to the adjustable chemistry of MOFs, the energetic parameters δ , $\epsilon_{\frac{1}{2}}$, and ϵ_{\triangle} can be tuned by changing the chemistry of the RMS-MOF, particularly the chemistry of the stations $\frac{1}{2}$ and of the macrocyclic wheel. For this reason, we define RMS-MOF material space to be the set of all parameters $(\delta, \epsilon_{\frac{1}{2}}, \epsilon_{\triangle})$, in the context of a particular gas, though we enforce (i) $\delta > 0$ to avoid model redundancy that, otherwise, arises from model

Table 2. Description of Model Parameters/Variables

type	description	symbol
material parameter	energy of gas molecule adsorbed on site $ $	$\epsilon_{ \!\!\!\!/ \!\!\!/}$
material parameter	energy of gas molecule adsorbed on site \triangle	$\epsilon_{ riangle}$
material parameter	energetic penalty for the wheel to occupy \triangle station	δ
microstate variable	position of the wheel $(w = 0 \Rightarrow \stackrel{L}{\Rightarrow}, w = 1 \Rightarrow \triangle)$	w
microstate variable	number of adsorbed gas molecules in the RMS-MOF unit cell	n
macrostate variable	chemical potential set by bulk gas phase	μ
macrostate variable	thermodynamic $\beta \equiv 1/(k_{\rm B}T)$ set by bulk gas phase	β

symmetry and (ii) ϵ_{\star} , ϵ_{\triangle} < 0 corresponding to attractive, as opposed to repulsive, site—gas interactions.

Classification of Material Space. We classify RMS-MOFs according to the relative gas—station and wheel—station affinities, i.e., according to their location in material space. These classifications, depicted in Figure 3a, are based on consideration of an RMS-MOF—gas system with n = 1 fixed (but w, the position of the wheel, can fluctuate in the nVT ensemble).

Case: $\epsilon_{\,\dot{\approx}} < \epsilon_{\,\dot{\triangle}}$, wheel—gas competition. If the gas has a higher affinity for the $\,\dot{\approx}\,$ site than for the $\,\dot{\triangle}$, adsorbed gas and the wheel compete for the $\,\dot{\approx}\,$ site. Three subcases of wheel—gas competition are ordered by increasing affinity of the gas for the $\,\dot{\approx}\,$ station:

Subcase: $\epsilon_{\triangle} < \epsilon_{\Rightarrow} + \delta$, wheel wins. The energetic preference of the gas for the \Rightarrow site over the \triangle site is insufficiently strong to offset the penalty for the wheel to occupy the \triangle station. In this subcase, the \Rightarrow station is the ground state of the wheel in both the fixed n=0 and fixed n=1 canonical ensembles.

Subcase: $\epsilon_{\frac{1}{2}} + \delta = \epsilon_{\triangle}$, detente. The energetic preference of the gas for the $\frac{1}{2}$ site over the $\frac{1}{2}$ site exactly offsets the energetic penalty for the wheel to reside on the $\frac{1}{2}$ station. In this subcase, the energies of the two microstates of the fixed n = 1 RMS-MOF-gas system are equal. Thus, in the fixed n = 1

canonical ensemble, the wheel shares residence equally between the \triangle and \Rightarrow stations.

Case: $e_{\star} = e_{\triangle}$, wheel–gas peace. The gas— \updownarrow attraction is equal to the gas— \bigtriangleup attraction. The gas is indifferent to which adsorption site it binds; hence, there is effectively no interaction between the gas and the wheel. A symmetric RMS-MOF that presents identical stations (" \updownarrow = \bigtriangleup ") exhibits wheel–gas peace.

Case $\epsilon_{\triangle} < \epsilon_{\Rightarrow}$: wheel—gas cooperation. The gas— \triangle interaction is more favorable than the gas— \Rightarrow interaction. Thus, the wheel and the gas energetically prefer opposite stations. We classify this as cooperation because, comparing the fixed n=0 and fixed n=1 canonical ensembles, the addition of a gas molecule increases the residence of the wheel on its preferred station, the \Rightarrow .

■ ADSORPTION PROPERTIES OF THE RMS-MOF

Grand-Canonical Partition Function. The grand-canonical partition function of the RMS-MOF unit cell in Figure 1b

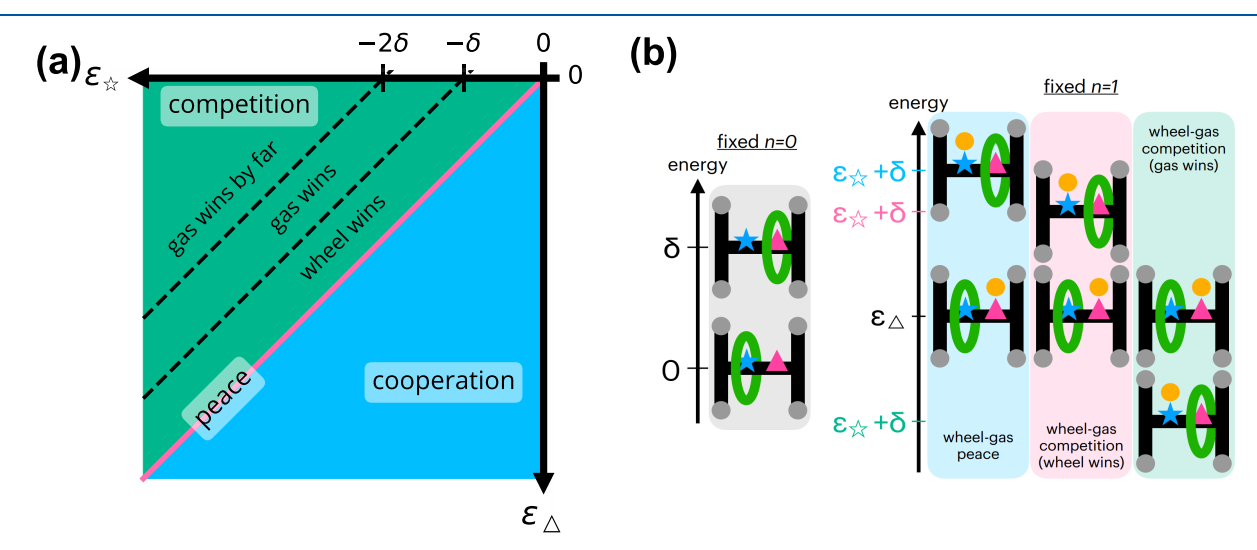


Figure 3. Classifying RMS-MOF—gas systems according to the relative gas—station and wheel—station affinities. (a) Slice of RMS-MOF material space with fixed δ , colored according to the classifications: wheel—gas competition, peace, and cooperation. (b) Depiction of the relative energies of the two microstates of the RMS-MOF for fixed n = 0 (left) and fixed n = 1 (right). The RMS-MOF classifications are based on the fixed n = 1 systems. Under wheel—gas competition, if the gas wins, the ground state of the wheel is on the \triangle in the fixed n = 1 canonical ensemble.

$$\xi(\mu, T) = \sum_{(w,n)\in\mathcal{W}\times\mathcal{N}} e^{-\beta E(w,n) + \beta \mu n}$$

$$= 1 + e^{-\beta\delta} + e^{\beta\mu} (e^{-\beta\epsilon} + e^{-\beta(\epsilon_{\pm} + \delta)})$$
(5)

with E(w, n) given by eq 4. The first two terms correspond to the two microstates with n = 0; the latter two correspond to n = 1.

Gas Adsorption. The expected number of adsorbed gas particles in the RMS-MOF is

$$\langle n \rangle (P, T) = \sum_{(w,n) \in \mathcal{W} \times \mathcal{N}} n \frac{e^{-\beta E(w,n) + \beta \mu n}}{\xi}$$
(6)

$$=\frac{K'\beta P}{1+K'\beta P} \tag{7}$$

with

$$K' = K'(T) \equiv \frac{1}{1 + e^{-\beta \delta}} e^{-\beta \epsilon_{\triangle}} + \frac{e^{-\beta \delta}}{1 + e^{-\beta \delta}} e^{-\beta \epsilon_{\pm}}$$
(8)

To arrive at eq 7, we substituted $e^{\beta\mu}$ with βP by treating the bulk gas phase as an ideal (lattice) gas (see Section S1). As each RMS-MOF unit cell in Figure 1b is independent, $\langle n \rangle$ represents the fraction of unit cells in a macroscopic RMS-MOF crystal that are occupied by a gas molecule.

The adsorption isotherm of the RMS-MOF, given in eq 7, exhibits a functional form/shape equivalent to that of a singlesite Langmuir model given in eq 2 and displayed in Figure 2b. The temperature-dependent, pseudo-Langmuir parameter K'in eq 8 describes the effective affinity of the gas for the RMS-MOF, with half of the RMS-MOF unit cells occupied when the density of the ideal gas phase $\beta P = 1/K'$. Intuitively, K' is a weighted average of the Langmuir parameters of a single- \triangle -site and a single- \Rightarrow -site MOF, $K_{\triangle} \equiv e^{-\beta \epsilon_{\triangle}}$, and $K_{\Rightarrow} \equiv e^{-\beta \epsilon_{\Rightarrow}}$, respectively; the weight $(1 + e^{-\beta \delta})^{-1}$ on K_{\triangle} is the probability that the wheel resides on ☆ when the RMS-MOF is empty of gas, thereby exposing the \triangle to the gas, while the weight on $K_{\underline{\diamond}}$ is the probability the wheel resides on \triangle when the RMS-MOF is empty of gas. However, we refer to K' as a pseudo-Langmuir parameter because its temperature dependence is not equivalent to a single- -site Langmuir model, $K_{\square}(T) \equiv e^{-\beta c_{\square}}$ (see Background: The Langmuir Adsorption Model section). An implication of this, which we explore later, is that gas adsorption in the RMS-MOF scales with temperature differently than in a Langmuir material.

Note, gas adsorption properties in the RMS-MOF are equivalent to the Langmuir adsorption model when:

- δ → ∞, as then the wheel is fixed at the ☆ station and the △ is invariably exposed to gas, giving a single-△-site Langmuir model.
- $\epsilon_{\frac{1}{2}} = \epsilon_{\triangle}$ (wheel-gas peace), as then the gas and the wheel effectively do not interact, giving a single- $\triangle = \frac{1}{2}$ -site Langmuir model.
- $\epsilon_{\triangle} = \epsilon_{\div} + 2\delta$, as then, we will later show, the entropy of the wheel is unaffected by the adsorption of gas, and gas adsorption in the RMS-MOF behaves as a single-site Langmuir model with a gas—site energy of interaction of $\epsilon_{\div} + \delta$.

Other than these cases, the temperature dependence of gas adsorption in the RMS-MOF model differs from a single-site

Langmuir model, owing to the translational entropy of the wheel that is altered by the adsorption of gas.

Position of the Wheel. The expected value of w, the probability that the wheel occupies the \triangle station, is

$$\langle w \rangle (P, T) = \sum_{(w,n) \in \mathcal{W} \times \mathcal{N}} w \frac{e^{-\beta E(w,n) + \beta \mu n}}{\xi}$$
 (9)

$$= \left(\frac{e^{-\beta\delta}}{1 + e^{-\beta\delta}}\right) \left(\frac{1 + e^{-\beta\epsilon_{+}}\beta P}{1 + K'\beta P}\right)$$
(10)

where K' is the temperature-dependent pseudo-Langmuir parameter given in eq 8.

We recover a two-state model for the wheel when P=0 and the RMS-MOF is empty of gas (fixed n=0), and when $P\to\infty$ and the RMS-MOF is certainly occupied by gas (fixed n=1). For fixed n=0, the wheel toggles between the $\not\simeq$ and \triangle stations with energies 0 and δ , respectively. For fixed n=1, the wheel toggles between the $\not\simeq$ and \triangle stations, in conjunction with the adsorbed gas toggling between the \triangle and $\not\simeq$ sites, respectively, with energies ε_{\triangle} and $\varepsilon_{\not\simeq}+\delta$, respectively. This is readily apparent after using eq 7 to write eq 10 as

$$\langle w \rangle = (1 - \langle n \rangle) \left(\frac{e^{-\beta \delta}}{1 + e^{-\beta \delta}} \right) + \langle n \rangle \left(\frac{e^{-\beta (\epsilon_{\pm} + \delta)}}{e^{-\beta \epsilon_{\triangle}} + e^{-\beta (\epsilon_{\pm} + \delta)}} \right)$$
(11)

As P increases from zero and gas fills the adsorption sites in the RMS-MOF, wheel–gas competition or cooperation affects the residency of the wheels. Both eqs 10 and 11 reveal three distinct cases illustrated in Figure 4. If the RMS-MOF exhibits wheel–gas competition $(e^{-\beta e_{\pm}} > K')$, more of the wheels reside on the \triangle station as gas adsorbs and "kicks" some wheels off of their energetically preferred \Rightarrow stations. If the RMS-MOF exhibits wheel–gas peace $(K' = e^{-\beta e_{\pm}})$, the adsorption of gas

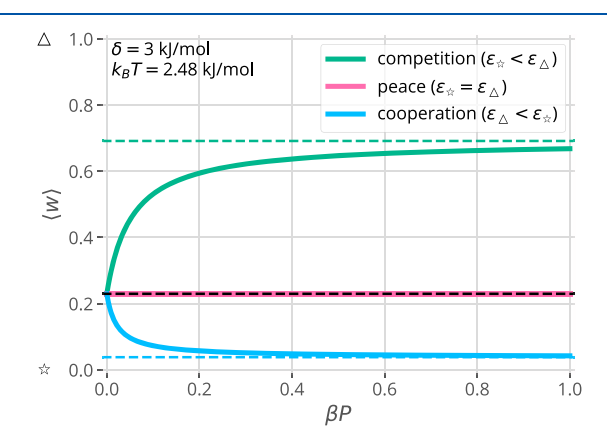


Figure 4. Fraction of the wheels in an RMS-MOF crystal that reside at their \triangle station, $\langle w \rangle$, as a function of the density of the ideal gas in which the RMS-MOF is immersed, βP , at fixed temperature (T=298 K), for three different RMS-MOFs. Because $\delta=3$ kJ/mol for all three RMS-MOFs, as $\beta P \to 0$, $\langle w \rangle \to \mathrm{e}^{-\beta\delta}/(1+\mathrm{e}^{-\beta\delta})$ for each MOF (black, dashed line). For the RMS-MOF with wheel–gas competition ($\epsilon_{\star}=-10$, $\epsilon_{\triangle}=-5$ kJ/mol), more of the wheels reside at the \triangle stations as gas adsorbs. For the RMS-MOF with wheel–gas peace ($\epsilon_{\star}=\epsilon_{\triangle}=-7$ kJ/mol), gas adsorption does not affect the position of the wheels. For the RMS-MOF with wheel–gas cooperation ($\epsilon_{\star}=-5$, $\epsilon_{\triangle}=-10$ kJ/mol), more of the wheels reside at the \Rightarrow stations as gas adsorbs. The green and blue dashed lines show $\langle w \rangle$ in the two-state model for fixed n=1 recovered by eq 11.

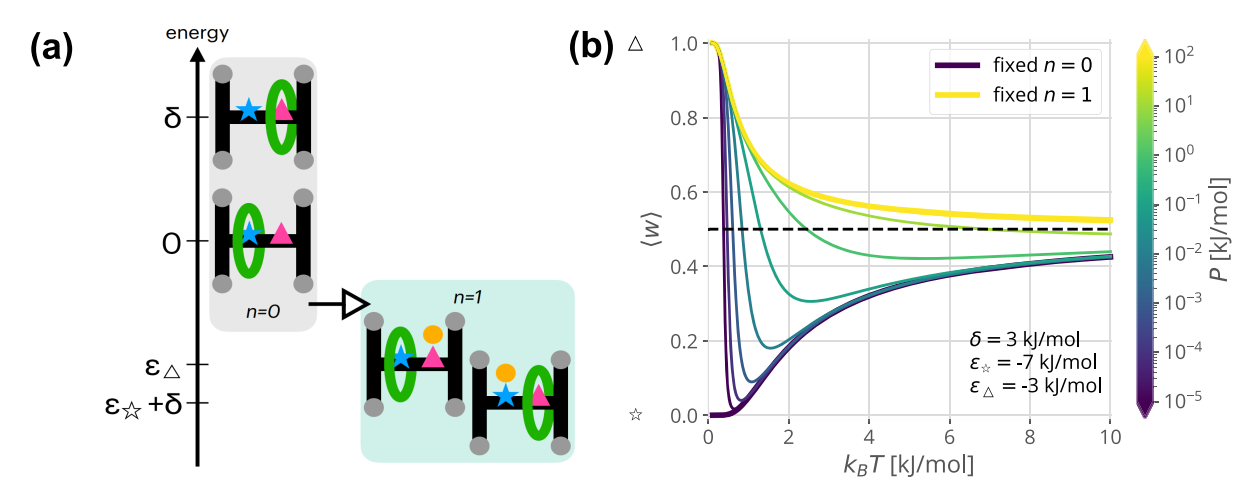


Figure 5. Under wheel—gas competition for the $\not\approx$ site, if the gas wins $(\epsilon_{\not\approx} + \delta < \epsilon_{\triangle})$, the position of the wheel in the RMS-MOF responds to temperature changes differently depending on the amount of gas adsorbed. (a) In the fixed n=0 RMS-MOF, the $\not\approx$ station is the ground state of the wheel $(\delta > 0)$. In the fixed n=1 RMS-MOF, the ground state of the wheel is on the \triangle so as to expose the $\not\approx$ to the gas $(\epsilon_{\not\approx} + \delta < \epsilon_{\triangle})$. Therefore, an increase in temperature increases wheel residence on the \triangle when the RMS-MOF is empty, but instead increases wheel residence on the $\not\approx$ when the RMS-MOF is full of gas. (b) Isobars of $\langle w \rangle$ (T,P) in eq 10, where color indicates pressure. The two thicker curves show $\langle w \rangle$ as a function of temperature for fixed n=0 (bottom) and fixed n=1 (top), corresponding with the two two-state models in (a). The isobars exhibit nonmonotonic temperature dependence as the RMS-MOF transitions between the two two-state models in (a) as gas fills/empties the RMS-MOF as it is cooled/warmed.

does not influence the position of the wheels, since the gas has no energetic preference for either the \triangle or \Leftrightarrow adsorption sites. If the RMS-MOF exhibits wheel–gas cooperation $(K' > e^{-\beta \varepsilon_{\pm}})$, more of the wheels reside on the \Leftrightarrow station as gas adsorbs and restricts the wheel from exploring its higher-energy state on the \triangle station while undergoing thermal fluctuations.

The perspective of the wheel as a transition between two two-state models as gas fills the RMS-MOF in eq 11 reveals that the direction of the temperature dependence of $\langle w \rangle$ can depend on the amount of gas adsorbed in the RMS-MOF. Consider the RMS-MOF empty of gas (fixed n = 0). The minimum-energy state of the wheel is the \Rightarrow station ($\delta > 0$). An increase in temperature thus induces the wheel to visit its higher-energy microstate, the \triangle station, more frequently. Now, consider the RMS-MOF full of gas (fixed n = 1). If ϵ_{\wedge} < an increase in temperature still increases the residence of the wheel on the \triangle station. However, if ϵ_{\pm} + δ < ϵ_{\triangle} (wheel–gas competition, gas wins), the \triangle station is the ground state for the wheel, so as to expose the \(\precedet\) site to the gas, and, instead, an increase in temperature increases the residence of the wheel on the ☆ station. Figure 5a illustrates this case of wheel-gas competition, where the gas wins and the ground state of the wheel switches upon adding or removing a gas molecule.

temperature, the wheel then increases its residence on the \triangle station with increasing temperature, like in the fixed n=0 case. In the high temperature limit, $\langle w \rangle = 0.5$ to maximize the entropy of the wheel. While we cannot speculate on a practical application, this nonmonotonic temperature dependence of $\langle w \rangle$, revealed by the model, is interesting and unexpected.

In Figure S1, we show $\langle w \rangle(P,T)$ and $\langle n \rangle(P,T)$ as heatmaps, for three different classes of RMS-MOFs.

How Gas Affects the Entropy of the Wheel. Under wheel—gas competition or cooperation, the adsorption of a gas molecule changes the configurational entropy of the wheel

$$S_{w} = -k_{\rm R}[\langle w \rangle \log \langle w \rangle + (1 - \langle w \rangle) \log(1 - \langle w \rangle)] \tag{12}$$

Figure 6 illustrates how $S_{\rm w}$ changes upon the addition of a gas molecule to the unit cell of the RMS-MOF, depending on its classification (see Figure 3a). The curve shows S_w at fixed n = 1a function of $\beta(\epsilon_{*}+\delta-\epsilon_{\triangle})$, given by eq 12 together with eq 11. Now, the xs show S_w at fixed n = 1 for different classes of RMS-MOFs, all with $\beta\delta$ = 3. For comparison, the solid black circle shows S_w at fixed n = 0 for all of the RMS-MOFs. Given $\delta > 0$, $S_{\rm w}$ is less than maximal when n = 0. Comparing $S_{\rm w}$ for fixed n = 0 and for fixed n = 1, arrive at the following conclusions. Under wheel-gas cooperation, the addition of a gas molecule decreases the entropy of the wheel because it increases the residence of the wheel on the ☆. Under wheelgas peace, the addition of a gas molecule has no effect on the entropy of the wheel. Under wheel-gas competition, the addition of a gas molecule increases the residence of the wheel on the \triangle station. If the wheel wins, the entropy of the wheel increases as a result. Under the detente case, the entropy of the wheel is maximized by the addition of a gas particle. If the gas wins, the entropy could either increase or decrease; the gas decreases S_w if it has a sufficient affinity for the \Rightarrow site (gas wins by far) so as to severely restrict the wheel from visiting the ☆ station. The addition of a gas molecule to the unit cell of the RMS-MOF increases the configurational entropy of the wheel if and only if $-2\delta < \epsilon_{\,\dot{\propto}} - \epsilon_{\,\dot{\triangle}} < 0$, the gray, shaded region in Figure 6.

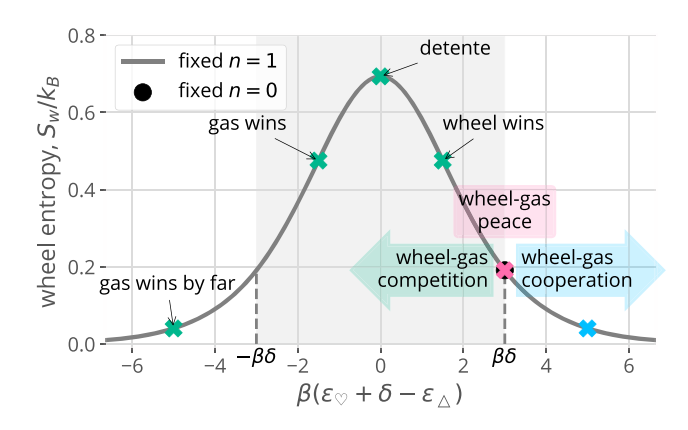


Figure 6. How gas affects the configurational entropy of the wheel, $S_{\rm w}$ in eq 12. The gray curve shows $S_{\rm w}$ at fixed n=1 as a function of $\beta(\varepsilon_{\not \approx}+\delta-\varepsilon_{\triangle})$. The x's mark $S_{\rm w}$ for fixed n=1 for RMS-MOFs of different classes, but all with $\beta\delta=3$. As a baseline, the black solid dot is $S_{\rm w}$ for fixed n=0 for all of the RMS-MOFs. Under wheel—gas cooperation, adsorbed gas reduces the entropy of the wheel. Under wheel—gas competition, adsorbed gas can increase or decrease the entropy of the wheel, depending on how strongly the gas prefers the $\not\approx$ -exposed RMS-MOF. In the gray-shaded region $-2\delta < \varepsilon_{\not\approx} - \varepsilon_{\triangle} < 0$, the addition of a gas molecule to the unit cell of the RMS-MOF increases the entropy of the wheel.

Energy Change Upon Gas Adsorption. The expected energy of the RMS-MOF-gas system is

$$\langle E \rangle (P, T) = \sum_{(w,n) \in W \times N} E(w, n) \frac{e^{-\beta E(w,n) + \beta \mu n}}{\xi}$$
$$= (1 - \langle n \rangle) \langle E \rangle_{n=0} + \langle n \rangle \langle E \rangle_{n=1}$$
(13)

where

$$\langle E \rangle_{n=0} = \delta \frac{e^{-\beta \delta}}{1 + e^{-\beta \delta}}$$

$$\langle E \rangle_{n=1} = \epsilon_{\triangle} \frac{e^{-\beta \epsilon_{\triangle}}}{e^{-\beta \epsilon_{\triangle}} + e^{-\beta(\epsilon_{+} + \delta)}}$$

$$+ (\epsilon_{+} + \delta) \frac{e^{-\beta(\epsilon_{+} + \delta)}}{e^{-\beta \epsilon_{\triangle}} + e^{-\beta(\epsilon_{+} + \delta)}}$$
(14)

are the expected energies of the RMS-MOF in the Canonical ensemble, with fixed n=0 and 1, respectively. eq 13 recovers the expected energy of the Langmuir model in eq 3 when $\delta=0$ and $\epsilon_{\dot{\pi}}=\epsilon_{\bigwedge}=\epsilon_{\bigcap}$.

The differential energy of adsorption is the change in energy of the (macroscopic) RMS-MOF system when a molecule adsorbs from the gas phase at a constant temperature. This quantity is important because it determines the heat released/consumed upon adsorption/desorption and thus temperature raises/drops in the adsorbent upon ad/desorption. Via eq 13, the differential energy of adsorption in our RMS-MOF is

$$\left(\frac{\partial \langle E \rangle}{\partial \langle n \rangle}\right)_{\mathrm{T}} = \langle E \rangle_{n=1} - \langle E \rangle_{n=1} \tag{15}$$

the difference between the expected energy in the fixed n=1 two-state model and the fixed n=0 two-state model. We rewrite eq 15 to separate the contributions from the wheel—station and gas—station interactions

$$\left(\frac{\partial \langle E \rangle}{\partial \langle n \rangle}\right)_{T} = \delta \left(\frac{e^{-\beta(\epsilon_{\pm} + \delta)}}{e^{-\beta\epsilon_{\triangle}} + e^{-\beta(\epsilon_{\pm} + \delta)}} - \frac{e^{-\beta\delta}}{1 + e^{-\beta\delta}}\right) + \epsilon_{\triangle} \frac{e^{-\beta\epsilon_{\triangle}}}{e^{-\beta\epsilon_{\triangle}} + e^{-\beta(\epsilon_{\pm} + \delta)}} + \epsilon_{\pm} \frac{e^{-\beta(\epsilon_{\pm} + \delta)}}{e^{-\beta\epsilon_{\triangle}} + e^{-\beta(\epsilon_{\pm} + \delta)}} \right)$$

$$(16)$$

The first term is the energy change due to the adsorbed gas altering the residency of the wheel, composed of wheel–station interactions. The second and third terms are the gas— \triangle and gas— \Rightarrow interactions, respectively, that appear when a gas molecule adsorbs into the RMS-MOF unit cell. Equation 16 reveals that the energy change of the wheel, as a result of the adsorbed gas altering the residency of the wheel, contributes to the heat released/consumed upon adsorption/desorption. Under wheel—gas competition (cooperation), the wheel contributes a positive (negative) term to the differential energy of adsorption, owing to the addition of a gas particle increasing residence of the wheel on the \triangle (\Rightarrow) station.

We remark that the differential energy of adsorption in eq 15 is not a function of $\langle n \rangle$ because the adsorption of gas molecule i in our model RMS-MOF crystal does not influence the free energy of adsorption of the next gas molecule i+1 that adsorbs.

COMPARISON TO A SINGLE-SITE LANGMUIR MODEL

We found the gas adsorption isotherm of the RMS-MOF, given in eq 7, to exhibit an identical functional form/shape as the single-site Langmuir adsorption isotherm displayed in Figure 2b. This raises the question: what possible advantage, for adsorption-based engineering processes, could an RMS-MOF have over an ordinary, rigid Langmuir MOF that lacks dynamic/flexible components? We next demonstrate two ways that the adsorption properties of the RMS-MOF fundamentally differ from a rigid, single-site Langmuir model that exhibits the same gas adsorption isotherm as the RMS-MOF at a reference temperature. Depending on the classification of the RMS-MOF, in the RMS-MOF:

- gas adsorption is more or less sensitive to changes in temperature. Key hint: the pseudo-Langmuir parameter K' in eq 8 is a more complicated function of temperature than the Langmuir parameter $K_{\square} \equiv \mathrm{e}^{-\beta \epsilon_{\square}}$ that appears in eq 2.
- more or less heat is released upon adsorption. Key hint: the wheel—station interaction contributes to the differential energy of adsorption in eq 16, whereas, in the Langmuir model, the differential energy of adsorption is entirely composed of the gas—site interaction.

For a suitable comparison between a given RMS-MOF and a single- \square -site Langmuir MOF at reference temperature T_0 , we assign the gas- \square interaction energy ϵ_\square such that the Langmuir parameter $K_\square \equiv \mathrm{e}^{-\beta\epsilon_\square}$ in eq 2 is equal to pseudo-Langmuir parameter K' of the RMS-MOF in eq 8. This equips the single- \square -site Langmuir material with an identical gas adsorption isotherm as the RMS-MOF at temperature T_0 . We refer to such a Langmuir material as the "cognate" Langmuir material to the RMS-MOF. Figure 7 shows the ϵ_\square that equates the Langmuir and pseudo-Langmuir parameters, $K_\square(T_0)$ =

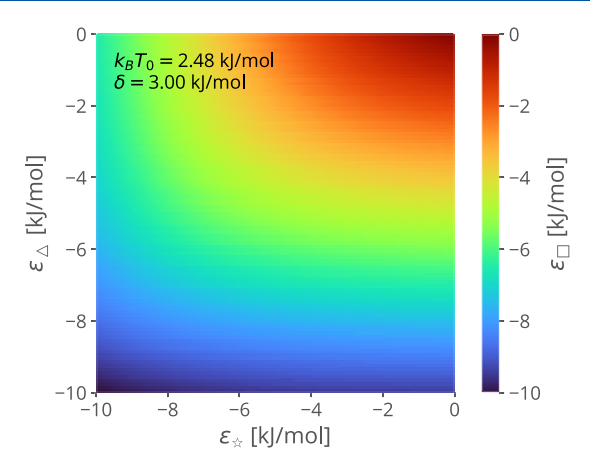


Figure 7. For a suitable comparison between a given RMS-MOF $(\delta, \epsilon_{\star}, \epsilon_{\triangle})$ and a single- \square -site Langmuir model, we assign the gas- \square interaction energy, ϵ_{\square} , to give the Langmuir MOF an adsorption isotherm identical to that of the RMS-MOF at a reference temperature T_0 . The plane shows a slice of material space with δ fixed. The color indicates ϵ_{\square} such that $K_{\square}(T_0) = \mathrm{e}^{-\epsilon_{\square}/(k_{\mathrm{B}}T_0)} = K'(T_0)$.

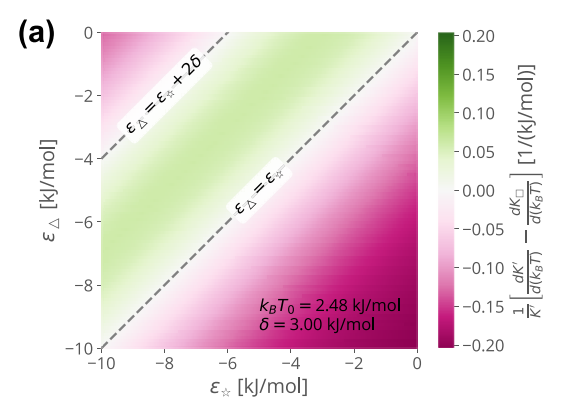
 $K'(T_0)$, and thus equates the adsorption isotherms at T_0 in the RMS-MOF and its cognate Langmuir material.

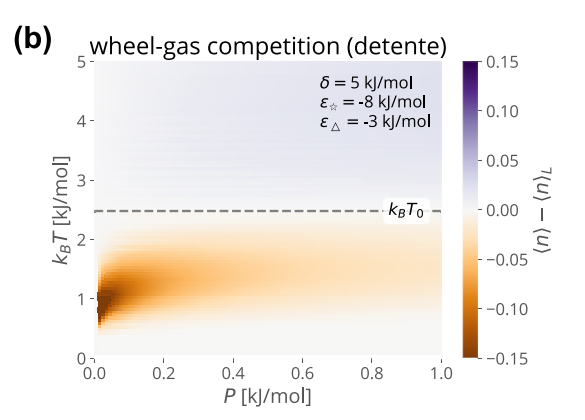
Temperature Sensitivity of Adsorption. Porous materials that exhibit either temperature-sensitive or temperature-insensitive adsorption are useful for engineering applications. Temperature-sensitive gas adsorption facilitates temperature-swing adsorption processes for gas storage and separations, where temperature increases are used to expel adsorbed gas from the adsorbent and regenerate it for another cycle. Temperature-insensitive gas adsorption minimizes pressure variations in adsorbed gas storage vessels exposed to a large range of temperatures. In addition, temperature-insensitive adsorption is desirable for adsorbents used in gas sensors that operate in a range of temperatures.

The difference between the temperature sensitivity of gas adsorption in an RMS-MOF and in its cognate single-site Langmuir material is

$$\left(\frac{\partial \langle n \rangle}{\partial T}\right)_{p} - \left(\frac{\partial \langle n \rangle_{L}}{\partial T}\right)_{p} = \langle n \rangle (1 - \langle n \rangle) \frac{1}{K'} \left(\frac{dK'}{dT} - \frac{dK_{\square}}{dT}\right)$$
(1)

which has the same sign as the difference between the temperature sensitivity of the pseudo-Langmuir parameter K' and the Langmuir parameter K_{\square} displayed in Figure 8a. Note $\frac{dK'}{dT}, \frac{dK_{\square}}{dT} \le 0$ for the parameters shown in Figure 8a. In the region $-2\delta < \epsilon_{\Rightarrow} - \epsilon_{\triangle} < 0$, gas adsorption in the RMS-MOF is less temperature sensitive than in the cognate Langmuir MOF. Outside this region, gas adsorption in the RMS-MOF is more temperature sensitive than in the cognate Langmuir MOF. Note for RMS-MOFs such that $-2\delta < \epsilon_{\alpha} - \epsilon_{\triangle} < 0$, the addition of a gas molecule increases the configurational entropy of the wheel (see Figure 6). Therefore, if the addition of gas increases (decreases) the entropy of the wheel, then gas adsorption in the RMS-MOF is less (more) temperature sensitive than in the cognate Langmuir material. The temperature sensitivity of adsorption in the RMS-MOF is equal to that in its cognate Langmuir MOF if ϵ_{\triangle} = ϵ_{\Rightarrow} or ϵ_{\triangle} = $\epsilon_{\frac{1}{2}}$ + 2 δ , since, then, the adsorption of gas does not alter the configurational entropy of the wheel.





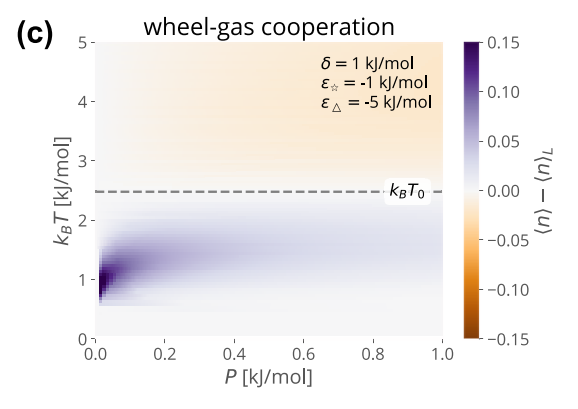


Figure 8. Comparing the temperature sensitivity of gas adsorption in the RMS-MOF to its cognate single-site Langmuir material, which presents an identical adsorption isotherm at reference temperature T_0 . (a) Plane is a slice of the RMS-MOF material space with δ fixed. The color depicts the normalized difference in the temperature sensitivity of the pseudo-Langmuir parameter of the RMS-MOF, K', and of the Langmuir parameter of the cognate Langmuir MOF, K_{\square} . RMS-MOFs in the green (pink) region exhibit less (more) temperature-sensitive adsorption than their cognate Langmuir materials. (b, c) For two different RMS-MOFs, the difference in their gas adsorption and the gas adsorption in their cognate Langmuir materials, as a function of pressure and temperature.

Figure 8b,8c displays the difference in gas adsorption between an RMS-MOF and its cognate Langmuir material in eq 17, for two different RMS-MOFs. At temperature T_0 , by definition of the cognate Langmuir material, the RMS-MOF and the Langmuir material adsorb the same amount of gas. The RMS-MOF in Figure 8b exhibits wheel—gas competition (detente). At any given pressure, it adsorbs less gas than the cognate Langmuir MOF at temperatures lower than T_0 and

more gas at temperatures higher than T_0 . Therefore, as a decrease and increase in temperature, respectively, induce the materials to uptake and expel gas, respectively, gas adsorption in this RMS-MOF is less temperature sensitive than in the cognate Langmuir material. In contrast, gas adsorption in an RMS-MOF with wheel—gas cooperation, as shown in Figure 8c, is more temperature sensitive than in the cognate Langmuir material

Differential Energy of Adsorption. Porous materials with either low or high differential energy of adsorption are useful for engineering applications. For gas storage and separations, porous materials that release minimal heat upon adsorption mitigate rises in temperature of the adsorbent bed upon gas charging, which detriment its adsorptive uptake. In contrast, porous materials that release a lot of heat upon adsorption are desired for thermal energy storage. So

Figure 9 compares the differential energy of adsorption in an RMS-MOF, given by eq 15, with the differential energy of

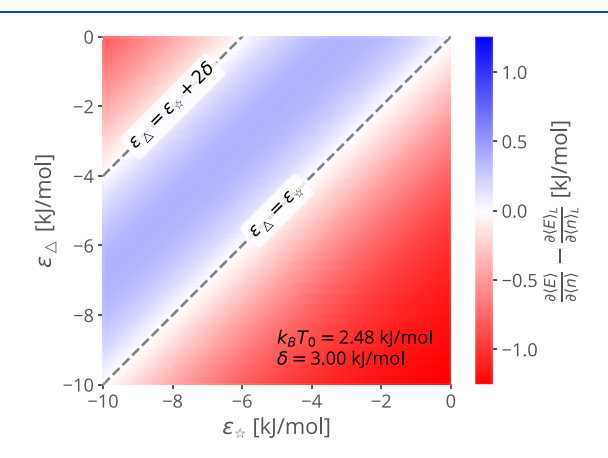


Figure 9. Comparing the differential energy of adsorption in RMS-MOFs to their cognate single-site Langmuir materials that present an identical adsorption isotherm at reference temperature T_0 . The plane is a slice of RMS-MOF material space with δ fixed. The color depicts the difference in the differential energy of adsorption in the RMS-MOF and in the Langmuir material. RMS-MOFs in the blue (red) region release less (more) heat upon gas adsorption than their cognate Langmuir materials.

adsorption in its cognate Langmuir MOF, ϵ_{\square} . Depending on the wheel–station and gas–site interactions, the differential energy of adsorption in the RMS-MOF can be more or less than in its cognate Langmuir material. If the addition of a gas particle increases the configurational entropy of the wheel (i.e., if $-2\delta < \epsilon_{\div} - \epsilon_{\triangle} < 0$), the differential energy of adsorption in the RMS-MOF is higher (i.e., less negative) than in the Langmuir material, and less heat is released upon adsorption in the RMS-MOF. On the other hand, if the addition of a gas particle decreases the configurational entropy of the wheel, the differential energy of adsorption in the RMS-MOF is lower (i.e., more negative) than in the Langmuir material, and more heat is released upon adsorption in the RMS-MOF. The differential energies of adsorption are equivalent when $\epsilon_{\div} = \epsilon_{\triangle}$ or $\epsilon_{\triangle} = \epsilon_{\pm} + 2\delta$.

Summary of RMS-MOF vs Langmuir Material. Though the gas adsorption isotherm in the model RMS-MOF exhibits an identical shape as a Langmuir adsorption model (see eqs 2 and 7), the temperature dependence of adsorption and the differential energy of adsorption differ between the RMS-MOF and its cognate Langmuir material that exhibits an identical

adsorption isotherm at a reference temperature T_0 . If the adsorption of a gas particle increases the configurational entropy of the wheel (i.e., if $-2\delta < \epsilon_{\frac{1}{2}} - \epsilon_{\triangle} < 0$), (i) gas adsorption is less temperature sensitive in the RMS-MOF and (ii) less heat is released upon gas adsorption in the RMS-MOF. On the other hand, if the adsorption of a gas particle decreases the entropy of the wheel, gas adsorption is more temperature sensitive and more heat is released upon adsorption. This entropic effect could be more dramatic when fully accounting for the degrees of freedom of a wheel in a bonafide RMS-MOF, such as translation along a continuum of states on the strut, circumrotation, and motion orthogonal to the axle.

■ GENERALIZING OUR RMS-MOF MODEL

To generalize our simple statistical mechanical model of an RMS-MOF, in Section S3, we allow multiple gas molecules to adsorb and interact in the unit cell of the RMS-MOF. We derive $\langle w \rangle$, $\langle n \rangle$, and $\langle E \rangle$ in terms of the adsorption properties of the two fixed-w RMS-MOFs, where the wheel is fixed on a station. Our key findings are:

- (Equation S17) The adsorption of gas increases the residence of the wheel on the ☆(△) station if the grand potential of the gas in the △-exposed (☆-exposed) RMS-MOF is lower than in the ☆-exposed (△-exposed) RMS-MOF.
- (Equation S19) An increase in temperature increases residence of the wheel on the \triangle (\updownarrow) station if the internal energy of the gas in the \triangle -exposed RMS-MOF is lower (higher) than the internal energy of the gas in the \updownarrow -exposed RMS-MOF plus the energetic penalty δ for the wheel to reside at the \triangle station.

DISCUSSION

Since 1918, when Langmuir introduced the single-site adsorption model, 47 many molecular-level adsorption models have been developed 47,51 to explain and predict adsorption phenomena from the bottom-up. The modular and adjustable nature of MOFs has expanded the scope of complexity we can integrate into porous materials, e.g., dynamic structures that respond to gas adsorption^{8–12} and, consequently, exhibit unique adsorption properties.¹⁴ We may be seeing a renaissance of simple, molecular-level statistical mechanical adsorption models to explain and predict exotic adsorption properties in these dynamic, gas-responsive materials, as exemplified by models to explain inflections in adsorption isotherms caused by gas-induced ligand rotation, 52 negative gas adsorption, 53,54 discontinuities in adsorption isotherms, 55 gasinduced framework expansion/contraction, 23,56-58 sharp steps in CO₂ adsorption via the formation of ammonium carbamate chains, 59 etc.

In this work, we developed a toy statistical mechanical model of gas adsorption in a metal—organic framework harboring a rotaxane molecular shuttle in its pores, an RMS-MOF. We formulated the simple abstraction of an RMS-MOF

in Figure 1b similar in spirit to the seminal Langmuir adsorption model, with the aim of qualitatively exploring the adsorption properties that could be imparted to a MOF by a shuttling wheel in its pores. Our model incorporates two salient features of an RMS-MOF: (i) the translational freedom of the shuttling wheel and (ii) wheel/gas competition for the stations/sites on the strut, and provides useful insights into how these features determine the amount of gas adsorbed, the residency of the wheel, and the differential energy of adsorption. While we found the gas adsorption isotherm of the RMS-MOF to exhibit an identical shape as a single-site Langmuir model, the shuttling wheel in the RMS-MOF affects (i) the temperature sensitivity of gas adsorption and (ii) the differential energy of adsorption. Compared to the cognate Langmuir material with an identical adsorption isotherm, depending on the interaction of the wheel and gas for the stations/sites, (i) gas adsorption can be more or less temperature sensitive and (ii) more or less heat can be released upon adsorption. Both properties are useful for engineering applications and emanate from the change in the configurational entropy of the shuttling wheel caused by the adsorption of gas. Finally, we found that if the gas fiercely competes the wheel for its favorite station, temperature changes affect the position of the wheel nonmonotonically at a fixed pressure.

Regarding the pursuit of RMS-MOFs for storing and separating gases, we have an "elephant in the room": the elephant is the macrocycle wheel wrapped around the strut of the MOF scaffold, and the room is the pore space in the MOF. This large macrocycle wheel occupies precious porosity that could otherwise host another gas molecule; the wheel imposes the limitation that fewer adsorption sites for gas molecules can be packed into a fixed volume of MOF. Therefore, the necessarily reduced porosity of a RMS-MOF as well as its synthetic complexity must be compensated for by its enhanced adsorption properties to see the application in gas storage and separations.

Our parsimonious toy model neglects many features of an RMS-MOF that could affect its adsorption properties, such as the continuum of wheel states along the strut, multiple gas molecules adsorbing in the unit cell and interacting with each other, adsorption sites on the MOF other than the two primary stations, interactions of gas molecules and wheels with those in neighboring unit cells, etc. Our simple model is a starting point for charting the properties that could be imparted into a MOF by a rotaxane molecular shuttle in its pores. It is a good approximation when the strut offers two distinct stations/sites that strongly attract the wheel/gas and thus dominate the thermodynamics.

Future work remains to chart further exotic adsorption properties offered by metal—organic frameworks harboring rotaxane molecular shuttles. To confirm our predictions herein, heroic experimental efforts are needed to synthesize a porous RMS-MOF, activate it, measure its gas adsorption properties, and characterize in situ the internal state of its macrocycle wheel as a function of gas adsorption. Thus far, only one MOF harboring a rotaxane shuttle has been synthesized. Some remaining knowledge gaps could be filled by extending our model. First, our toy model could be decorated with complexity to account for other molecular features that can be engineered into RMS-MOFs: (i) a radially asymmetric macrocycle on the rotaxane, whose rotational conformations expose different functional groups to the stations (see ref 44),

(ii) multiple stations [and, thus, adsorption sites] on the axle of the rotaxane, (iii) multiple macrocycle wheels threaded around the axle of the rotaxane, 60 (iv) arranging molecular shuttles in a MOF in a more complicated topology to allow coupling between neighboring molecular shuttles (inspired by ref 61), and (v) allowing multiple gas molecules to adsorb in a unit cell. Outside the context of MOFs, Sevick and Williams developed and analyzed a statistical mechanical model of radially asymmetric wheels⁶² [case (i)] and multiple wheels⁶³⁻⁶⁵ [case (iii)] in a rotaxane molecular shuttle and uncovered interesting behavior. Second, analyzing our model RMS-MOF immersed in a mixture of gases could reveal enhanced selectivity arising from the molecular shuttle. Intriguingly, gas adsorption in the RMS-MOF in Figure 1b bears some resemblance to biomolecular recognition, where, e.g., a ligand binds to a protein and induces a shift in its conformational ensemble.⁶⁶ Third, modeling can shed light on the interplay of external stimuli and adsorption in MOFs with stimuli-responsive rotaxanes⁶⁷ integrated into them. Fourth, atomistic models of RMS-MOFs could explore the practical constraints on material space $(\delta, \epsilon_{\star}, \epsilon_{\wedge})$ and suggest explicit RMS-MOF chemistry to pursue for anomalous adsorption properties.

ASSOCIATED CONTENT

Supporting Information

The Supporting Information is available free of charge at https://pubs.acs.org/doi/10.1021/acs.langmuir.0c02839.

Ideal lattice gas derivation; visualizations of $\langle w \rangle (P, T)$ and $\langle n \rangle (P, T)$; and our generalized RMS-MOF model (PDF)

AUTHOR INFORMATION

Corresponding Authors

David Roundy — Department of Physics, Oregon State University, Corvallis, Oregon 97331, United States; Email: roundyd@physics.oregonstate.edu

Cory M. Simon — School of Chemical, Biological, and Environmental Engineering, Oregon State University, Corvallis, Oregon 97331, United States; orcid.org/0000-0002-8181-9178; Email: Cory.Simon@oregonstate.edu

Author

Jonathan Carney — Department of Physics, Oregon State University, Corvallis, Oregon 97331, United States

Complete contact information is available at: https://pubs.acs.org/10.1021/acs.langmuir.0c02839

Note:

The authors declare no competing financial interest.

ACKNOWLEDGMENTS

C.M.S. acknowledges the National Science Foundation for support under Grant No. 1920945. Thanks to Adrian Henle for the drawing in Figure 1a.

REFERENCES

(1) Morris, R. E.; Wheatley, P. S. Gas storage in nanoporous materials. *Angew. Chem., Int. Ed.* **2008**, 47, 4966–4981.

(2) Li, J.-R.; Kuppler, R. J.; Zhou, H.-C. Selective gas adsorption and separation in metal-organic frameworks. *Chem. Soc. Rev.* **2009**, 38, 1477–1504.

- (3) Kreno, L. E.; Leong, K.; Farha, O. K.; et al. Metal-organic framework materials as chemical sensors. *Chem. Rev.* **2012**, *112*, 1105–1125.
- (4) Yaghi, O. M.; O'Keeffe, M.; Ockwig, N. W.; et al. Reticular synthesis and the design of new materials. *Nature* **2003**, *423*, 705–714.
- (5) Furukawa, H.; Cordova, K. E.; O'Keeffe, M.; et al. The chemistry and applications of metal-organic frameworks. *Science* **2013**, *341*, No. 1230444.
- (6) Moghadam, P. Z.; Li, A.; Wiggin, S. B.; et al. Development of a Cambridge Structural Database Subset: A Collection of Metal—Organic Frameworks for Past, Present, and Future. *Chem. Mater.* **2017**, 29, 2618–2625.
- (7) Deng, H.; Olson, M. A.; Stoddart, J. F.; et al. Robust dynamics. *Nat. Chem.* **2010**, *2*, 439–443.
- (8) Horike, S.; Shimomura, S.; Kitagawa, S. Soft porous crystals. *Nat. Chem.* **2009**, *1*, 695–704.
- (9) Schneemann, A.; Bon, V.; Schwedler, I.; et al. Flexible metalorganic frameworks. *Chem. Soc. Rev.* **2014**, *43*, 6062–6096.
- (10) Coudert, F.-X. Responsive metal-organic frameworks and framework materials: under pressure, taking the heat, in the spotlight, with friends. *Chem. Mater.* **2015**, 27, 1905–1916.
- (11) Chang, Z.; Yang, D.-H.; Xu, J.; et al. Flexible metal-organic frameworks: recent advances and potential applications. *Adv. Mater.* **2015**, 27, 5432–5441.
- (12) Lee, J. H.; Jeoung, S.; Chung, Y. G.; et al. Elucidation of flexible metal-organic frameworks: Research progresses and recent developments. *Coord. Chem. Rev.* **2019**, *389*, 161–188.
- (13) Krause, S.; Hosono, N.; Kitagawa, S. Chemistry of Soft Porous Crystals-Structural Dynamics and Gas Adsorption Properties. *Angew. Chem., Int. Ed.* **2020**, *132*, 15438–15456.
- (14) Coudert, F.-X.; Evans, J. D. Nanoscale metamaterials: Meta-MOFs and framework materials with anomalous behavior. *Coord. Chem. Rev.* **2019**, 388, 48–62.
- (15) Winston, E. B.; Lowell, P. J.; Vacek, J.; et al. Dipolar molecular rotors in the metal-organic framework crystal IRMOF-2. *Phys. Chem. Chem. Phys.* **2008**, *10*, 5188–5191.
- (16) Krause, S.; Evans, J. D.; Bon, V.; et al. Towards general network architecture design criteria for negative gas adsorption transitions in ultraporous frameworks. *Nat. Commun.* **2019**, *10*, No. 3632.
- (17) Serre, C.; Millange, F.; Thouvenot, C.; et al. Very Large Breathing Effect in the First Nanoporous Chromium (III)-Based Solids: MIL-53 or Cr^{III} (OH)· $\{O_2\text{C-C}_6H_4\text{-CO}_2\}$ · $\{HO_2\text{C-C}_6H_4\text{-CO}_2H\}_x$ · H_2O_y . J. Am. Chem. Soc. **2002**, 124, 13519–13526.
- (18) Kitaura, R.; Seki, K.; Akiyama, G.; et al. Porous Coordination-Polymer Crystals with Gated Channels Specific for Supercritical Gases. *Angew. Chem., Int. Ed.* **2003**, 42, 428–431.
- (19) Elsaidi, S. K.; Mohamed, M. H.; Simon, C. M.; et al. Effect of ring rotation upon gas adsorption in SIFSIX-3-M (M= Fe, Ni) pillared square grid networks. *Chem. Sci.* **2017**, *8*, 2373–2380.
- (20) Mason, J. A.; Oktawiec, J.; Taylor, M. K.; et al. Methane storage in flexible metal-organic frameworks with intrinsic thermal management. *Nature* **2015**, 527, 357–361.
- (21) Krause, S.; Bon, V.; Senkovska, I.; et al. A pressure-amplifying framework material with negative gas adsorption transitions. *Nature* **2016**, 532, 348.
- (22) Boutin, A.; Springuel-Huet, M.-A.; Nossov, A.; et al. Breathing Transitions in MIL-53 (Al) Metal-Organic Framework Upon Xenon Adsorption. *Angew. Chem., Int. Ed.* **2009**, *48*, 8314–8317.
- (23) Ghysels, A.; Vanduyfhuys, L.; Vandichel, M.; et al. On the thermodynamics of framework breathing: A free energy model for gas adsorption in MIL-53. *J. Phys. Chem. C* **2013**, *117*, 11540–11554.
- (24) Evans, J. D.; Bocquet, L.; Coudert, F.-X. Origins of negative gas adsorption. *Chem* **2016**, *1*, 873–886.
- (25) Choi, H. J.; Dinca, M.; Long, J. R. Broadly hysteretic H₂ adsorption in the microporous metal- organic framework Co(1, 4-benzenedipyrazolate). *J. Am. Chem. Soc.* **2008**, 130, 7848–7850.

- (26) Chang, K.; Talu, O. Behavior and performance of adsorptive natural gas storage cylinders during discharge. *Appl. Therm. Eng.* **1996**, 16, 359–374.
- (27) Coskun, A.; Banaszak, M.; Astumian, R. D.; et al. Great expectations: can artificial molecular machines deliver on their promise. *Chem. Soc. Rev.* **2012**, *41*, 19–30.
- (28) Martinez-Bulit, P.; Stirk, A. J.; Loeb, S. J. Stirk Rotors, Motors, and Machines Inside Metal-Organic Frameworks. *Trends Chem.* **2019**, 1, 588–600.
- (29) Krause, S.; Feringa, B. L. Towards artificial molecular factories from framework-embedded molecular machines. *Nat. Rev. Chem.* **2020**, *4*, 550–562.
- (30) Stoddart, J. F. The chemistry of the mechanical bond. *Chem. Soc. Rev.* **2009**, *38*, 1802–1820.
- (31) Bruns, C. J.; Stoddart, J. F. The Nature of the Mechanical Bond: From Molecules to Machines; John Wiley & Sons, 2016.
- (32) Anelli, P. L.; Spencer, N.; Stoddart, J. F. A molecular shuttle. *J. Am. Chem. Soc.* **1991**, *113*, 5131–5133.
- (33) Balzani, V.; Credi, A.; Raymo, F. M.; et al. Artificial molecular machines. *Angew. Chem., Int. Ed.* **2000**, *39*, 3348–3391.
- (34) Abendroth, J. M.; Bushuyev, O. S.; Weiss, P. S.; et al. Controlling motion at the nanoscale: rise of the molecular machines. *ACS Nano* **2015**, *9*, 7746–7768.
- (35) Loeb, S. J. Metal-organic rotaxane frameworks; MORFs. *Chem. Commun.* **2005**, 1511–1518.
- (36) Zhu, K.; O'Keefe, C. A.; Vukotic, V. N.; et al. A molecular shuttle that operates inside a metal-organic framework. *Nat. Chem.* **2015**, *7*, 514–519.
- (37) Coskun, A.; Hmadeh, M.; Barin, G.; et al. Metal-Organic Frameworks Incorporating Copper-Complexed Rotaxanes. *Angew. Chem., Int. Ed.* **2012**, *51*, 2160–2163.
- (38) Farahani, N.; Zhu, K.; O'Keefe, C. A.; et al. Thermally Driven Dynamics of a Rotaxane Wheel about an Imidazolium Axle inside a Metal-Organic Framework. *ChemPlusChem* **2016**, *81*, 836–841.
- (39) Vukotic, V. N.; Loeb, S. J. Coordination polymers containing rotaxane linkers. *Chem. Soc. Rev.* **2012**, *41*, 5896–5906.
- (40) Zhu, K.; Vukotic, V. N.; O'Keefe, C. A.; et al. Metal-organic frameworks with mechanically interlocked pillars: controlling ring dynamics in the solid-state via a reversible phase change. *J. Am. Chem. Soc.* **2014**, *136*, 7403–7409.
- (41) Vukotic, V. N.; O'Keefe, C. A.; Zhu, K.; et al. Mechanically interlocked linkers inside metal-organic frameworks: effect of ring size on rotational dynamics. *J. Am. Chem. Soc.* **2015**, *137*, 9643–9651.
- (42) Loeb, S. J. Rotaxanes as ligands: from molecules to materials. *Chem. Soc. Rev.* **2007**, *36*, 226–235.
- (43) Knight, L. K.; Vukotic, V. N.; Viljoen, E.; et al. Eliminating the need for independent counterions in the construction of metalorganic rotaxane frameworks (MORFs). *Chem. Commun.* **2009**, 5585–5587.
- (44) Baggi, G.; Loeb, S. J. Rotationally Active Ligands: Dialing-Up the Co-conformations of a [2] Rotaxane for Metal Ion Binding. *Angew. Chem., Int. Ed.* **2016**, *55*, 12533–12537.
- (45) Yang, Y.-D.; Fan, C.-C.; Rambo, B. M.; et al. Multicomponent Self-Assembled Metal-Organic [3] Rotaxanes. *J. Am. Chem. Soc.* **2015**, 137, 12966–12976.
- (46) Saura-Sanmartin, A.; Martinez-Cuezva, A.; Bautista, D.; et al. Copper-Linked Rotaxanes for the Building of Photoresponsive Metal Organic Frameworks with Controlled Cargo Delivery. *J. Am. Chem. Soc.* **2020**, *142*, 13442–13449.
- (47) Swenson, H.; Stadie, N. P. Langmuiras theory of adsorption: A centennial review. *Langmuir* **2019**, *35*, 5409–5426.
- (48) Torres-Knoop, A.; Poursaeidesfahani, A.; Vlugt, T. J.; et al. Behavior of the enthalpy of adsorption in nanoporous materials close to saturation conditions. *J. Chem. Theory Comput.* **2017**, *13*, 3326–3339.
- (49) Chang, K.; Talu, O. Behavior and performance of adsorptive natural gas storage cylinders during discharge. *Appl. Therm. Eng.* **1996**, 16, 359–374.

- (50) Kohler, T.; Müller, K. Influence of different adsorbates on the efficiency of thermochemical energy storage. *Energy Sci. Eng.* **2017**, *5*, 21–29
- (51) Hill, T. L. An Introduction to Statistical Thermodynamics; Courier Corporation, 1986.
- (52) Simon, C. M.; Braun, E.; Carraro, C.; et al. Statistical mechanical model of gas adsorption in porous crystals with dynamic moieties. *Proc. Natl. Acad. Sci. U.S.A.* **2017**, *114*, E287–E296.
- (53) Manos, G.; Dunne, L. Predicting the features of methane adsorption in large pore metal-organic frameworks for energy storage. *Nanomaterials* **2018**, *8*, No. 818.
- (54) Evans, J. D.; Krause, S.; Kaskel, S.; et al. Exploring the thermodynamic criteria for responsive adsorption processes. *Chem. Sci.* **2019**, *10*, 5011–5017.
- (55) Dunne, L. J.; Manos, G. Exact matrix treatment of an osmotic ensemble model of adsorption and pressure induced structural transitions in metal organic frameworks. *Dalton Trans.* **2016**, *45*, 4213–4217.
- (56) Dunne, L. J.; Manos, G. Statistical mechanics of binary mixture adsorption in metal-organic frameworks in the osmotic ensemble. *Philos. Trans. R. Soc., A* **2018**, 376, No. 20170151.
- (57) Triguero, C.; Coudert, F.-X.; Boutin, A.; et al. Mechanism of breathing transitions in metal-organic frameworks. *J. Phys. Chem. Lett.* **2011**, *2*, 2033–2037.
- (58) Witman, M.; Ling, S.; Stavila, V. et al. Design Principles for the Ultimate Gas Deliverable Capacity Material: Nonporous to Porous Deformations Without Volume Change 2020.
- (59) Kundu, J.; Stilck, J. F.; Lee, J.-H.; et al. Cooperative gas adsorption without a phase transition in metal-organic frameworks. *Phys. Rev. Lett.* **2018**, *121*, No. 015701.
- (60) Fang, L.; Olson, M. A.; Benítez, D.; et al. Mechanically bonded macromolecules. *Chem. Soc. Rev.* **2010**, *39*, 17–29.
- (61) Reddy, P.; Sevick, E. M.; Williams, D. R. Triangular cyclic rotaxanes: Size, fluctuations, and switching properties. *Proc. Natl. Acad. Sci. U.S.A.* **2018**, *115*, 9367–9372.
- (62) Sevick, E. M.; Williams, D. R. Conformational isomers of linear rotaxanes. *J. Chem. Phys.* **2014**, *141*, No. 114904.
- (63) Sevick, E. M.; Williams, D. Piston-rotaxanes as molecular shock absorbers. *Langmuir* **2010**, *26*, 5864–5868.
- (64) Sevick, E. M.; Williams, D. R. A piston-rotaxane with two potential stripes: Force transitions and yield stresses. *Molecules* **2013**, *18*, 13398–13409.
- (65) Sevick, E. M.; Williams, D. R. A Two-Stroke, Two-Cylinder Piston Rotaxane Motor. *ChemPhysChem* **2016**, 17, 1927–1933.
- (66) Boehr, D. D.; Nussinov, R.; Wright, P. E. The role of dynamic conformational ensembles in biomolecular recognition. *Nat. Chem. Biol.* **2009**, *5*, 789.
- (67) Xue, M.; Yang, Y.; Chi, X.; et al. Development of pseudorotaxanes and rotaxanes: from synthesis to stimuli-responsive motions to applications. *Chem. Rev.* **2015**, *115*, 7398–7501.